Mechanical Flux-Weakening for a Surface Permanent Magnet Machine with Split Rotor

Jonida Cekani
Dept. of Astronautical, Electrical and Energy Engineering
Sapienza University of Rome
Rome, Italy
jonida.cekani@uniroma1.it

Fabio Giulii Capponi
Dept. of Astronautical, Electrical and Energy Engineering
Sapienza University of Rome
Rome, Italy
fabio.giuliicapponi@uniroma1.it

Federico Caricchi
Dept. of Astronautical, Electrical and Energy Engineering
Sapienza University of Rome
Rome, Italy
federico.caricchi@uniroma1.it

***Abstract*— This paper presents a mechanical flux-weakening solution for Surface Permanent Magnet machines. In particular, a split rotor configuration (two independent rotor sections that can be phase-shifted) is discussed, in which the rotors shifting is achieved through a torque component generated inside the machine, without the need for any external actuation. The analysis demonstrates that the theoretical constant power speed range is infinite. The reliability of the active actuation through the shifting torque promises for a very wide achievable constant power speed range in practice.**

Keywords—Mechanical flux weakening, split rotor, Constant Power Speed Range, Surface Permanent Magnet machines

I. INTRODUCTION

The rapid evolution of technology is accompanied by the demand for electrical machines with higher power ratings. This, together with the existing space constraints, leads to researching highly efficient, high torque density machines, which can deliver their power over a wide speed range. For example, traction drives and integrated starter/alternators in the automotive industry necessitate wide constant power speed ranges (CPSRs), commonly in the range of 10:1 [1].

Permanent magnet machines are widespread in the industry, merit of their high torque density and efficiency. However, the CPSR of surface permanent magnet (SPM) machines that use the traditional electrical flux-weakening (EFW) is generally very limited because this topology is characterized by a low stator inductance. The addition of external inductors or the adoption of fractional slot concentrated windings [2] would improve the CPSR, but at the cost of a decrease in the power factor and a necessity for voltage oversizing of the inverter [3].

In general, when it comes to a wide CPSR, interior permanent magnet (IPM) machines are preferred. By improving their saliency ratio (i.e., increasing the difference between the q- and d-axis inductance, which is directly proportional to the reluctance torque), the permanent magnet requirements can be lowered [4], hence reducing the required flux weakening d-axis current. In [5], it is demonstrated that inverse saliency PM machines might achieve up to approximately 5:1 CPSR, and possibly even wider CPSR could be achieved by normal saliency PM machines. However, such very high saliency ratios cannot be practically realized with the conventional two- or three-barrier IPM rotor designs, thus the system is correspondingly penalized by the high complexity and cost. Moreover, IPM topologies present a high risk of irreversible demagnetization of the PMs, especially at high operating temperatures.

Hybrid excitation PM machines include a separate DC field supplier that can regulate the total magnetization level, leading to the possibility of a very wide speed range [6]. Yet, this topology comes with an increased complexity, lower efficiency, lower power density and, in some cases, with a high risk of irreversible demagnetization.

Another important aspect to be considered when designing the flux-regulation method is the overvoltage-proofing. Specifically, in case of a power outage or fault during high-speed operation, EFW cannot be applied, leading to uncontrolled generator operation.

On the other side, a significant CPSR can be obtained through mechanical flux-weakening (MFW), which relies solely on the physical modification of the magnetic circuitry in the machine, avoiding the consumption of current for the flux-regulation. Thus, a higher efficiency, enhanced safety and an overall wider CPRS can be expected. In [7], MFW arrangements were classified in three categories: with moveable magnetic leakage elements, [8-13], with varying airgap length, [14-18] and with moveable stator/rotor/-sections [19-23]. They were further classified in self-actuated arrangements (typically the centrifugal force provides the modification of the magnetic circuitry), [8-10], [19], [21], [22], and active arrangements (separate actuators provide the modification) [11-18], [20], [23]. The conclusions were that the self-actuated MFW is highly efficient, but of limited accuracy and dynamics. The active MFW offers better accuracy and dynamic behavior, but the problem of high system complexity remains. Furthermore, [7] highlighted that, in the majority of MFW examples, the process of flux-regulation modifies the magnetic energy stored in the system. Consequently, significant force is necessary to suppress the magnetic interaction that rises during the flux-regulation, and thus, the MFW of these examples is accompanied by a decrease in efficiency and a high complexity/cost.

As an alternative, the axial flux PM machines in [19], [20], [21] demonstrate flux linkage regulation using a phase-shifting technique that does not change the magnetic stored energy and therefore requires negligible power. Fig. 1 demonstrates the MFW arrangement of [19]. In the aligned position A (i.e., when same polarity magnets face each other), all the flux lines from the PMs link with the stator winding. When a phase-shift exists between the rotors (B), some flux lines do not close around the stator winding, thus leading to reduced flux linkage. In order to perform the phase-shifting, either passive mechanical devices located on the rotor, [19], [21] or active ones on the stator [20] are employed. However, the presence of mechanical devices increases the complexity of the arrangements, limits the dynamics, and deteriorates the accuracy of the flux regulation.

2022 IEEE Energy Conversion Congress and Exposition (ECCE) | 978-1-7281-9387-8/22/$31.00 ©2022 IEEE | DOI: 10.1109/ECCE50734.2022.9947662

978-1-7281-9387-8/22/$31.00 ©2022 IEEE

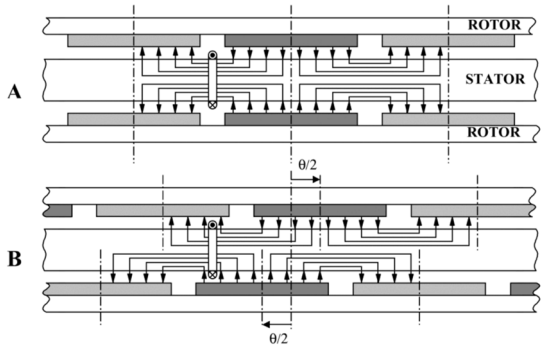

Fig. 1. Mechanical weakening of flux linkage via regulation of the angular phase-shift between the two PM rotor discs: (A) aligned rotors and (B) phase-shifted rotors. [19]

This article presents an innovative machine solution for MFW, in which the phase-shift of the rotors is adjusted using the electromagnetic torque generated inside the machine, through the d-axis current, without any external device. Even if the same solution can be applied to both axial- and radial-flux SPM machines, this article focuses on the radial-flux solution. The proposed machine is derived from a traditional SPM configuration (from this point onwards referred to as the base machine), in which a split rotor (SR) replaces the original one, while the stator remains the same. It should be noted here that the aim of this paper is to present the conceptual idea and, as consequence, the resulting machine is not optimized.

The SR configuration consists of two identical rotor sections (R1 and R2), separated by an in-between spacer airgap, each of them connected to a separate shaft, as in the schematic cross-section of Fig. 2. A standard automotive differential gearbox acts as a synchronizer, allowing R1 and R2 to shift one with respect to the other, while at the same time rotating together in the same direction. The gearbox makes it possible to sum the torques at the two shafts onto the output shaft, which is connected to the load. Both the replacement of the phase-shifting mechanical devices in [19-21] with the internally produced shifting torque, and the selection of a radial-flux topology (widely spread in the industry), are expected to contribute positively to the feasibility and manufacturability of the proposed solution.

In section II of this paper, the main equations that define the torque capability of the machine are discussed. In III, a comparison is made between the base machine with EFW and the SR one with MFW, focusing on the torque density and the obtainable CPSR. The performances of the SR solution are verified in IV, through finite elements simulations.

II. SR Machine with MFW

In the SR machine, the total no load flux linked with the stator winding, λ_{PM}, is the vector sum of the PM flux linkage contributions from each of the rotor sections λ_{PM1} and λ_{PM2}.

If these sections are equal, then $\lambda_{PM1} = \lambda_{PM2}$. Assuming a purely sinusoidal field distribution, when the rotor sections are aligned (same-polarity magnets face each other, as in Fig. 3), the vector sum becomes an algebraic sum, resulting in maximum flux linkage, $\lambda_{PM,algn} = \lambda_{PM1} + \lambda_{PM2}$. If R1 and R2 are out of alignment (see Fig. 4) by an electrical phase-shift angle α_{el}, the total PM flux linkage is decreased and MFW can be obtained, as proved by the synchronous frame vector diagram of Fig. 5:

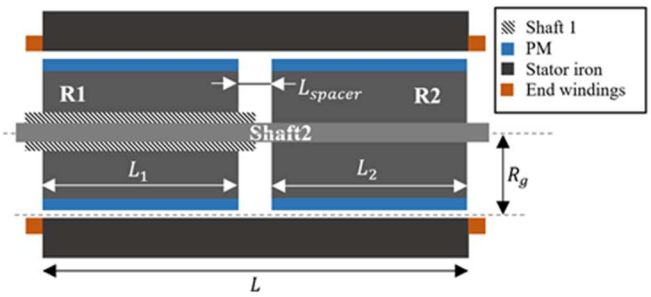

Fig. 2. Schematic cross-section representation of the SR machine

$$\lambda_{PM} = \lambda_{PM1}\cos(\alpha_{el}) + \lambda_{PM2}\cos(\alpha_{el}) = \lambda_{PM,algn}\cos(\alpha_{el}) \quad (1)$$

Based on (1), an angle $\alpha_{el} = \pi/2$ (opposite-polarity magnets face each other) nulls the PM flux linkage. The described MFW technique can keep the induced voltage constant in the CPSR region by increasing the phase-shift with speed, according to the following formula:

$$E = \omega_e\lambda_{PM} = \omega_e\lambda_{PM,algn}\cos(\alpha_{el}) = E_{max} \quad (2)$$

$$\alpha_{el} = \arccos\left(\frac{E_{max}}{\omega_e\lambda_{PM,algn}}\right) \quad (3)$$

The gearbox enables the summation of the torque contributions from each rotor section, resulting in the total motoring torque of the SR machine:

$$T = \frac{3}{2}P\left(\lambda_{R1d}i_q - \lambda_{R1q}i_d\right) + \frac{3}{2}P\left(\lambda_{R2d}i_q - \lambda_{R2q}i_d\right) \quad (4)$$

Since the q-axis components of the flux linkage contributions of the two rotor sections are equal and opposite (Fig. 5), it follows that:

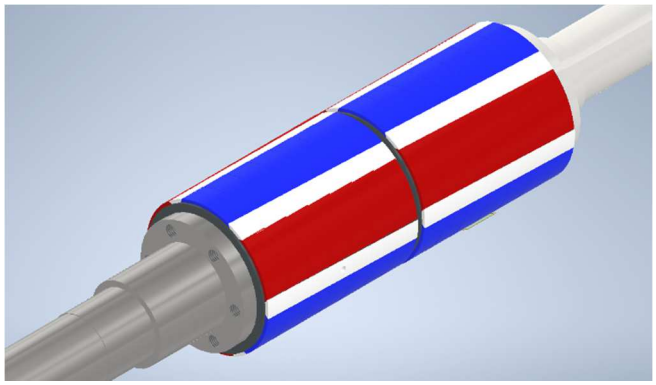

Fig. 3. 3D view of the SR machine for aligned rotor sections (stator not shown)

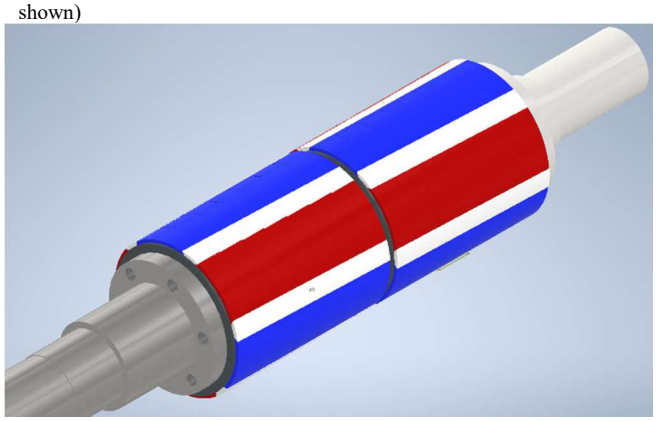

Fig. 4. 3D view of the SR machine for phase-shifted rotor sections (stator not shown)

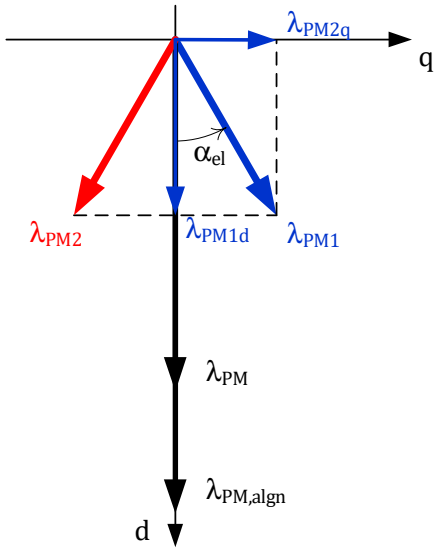

Fig. 5. Diagram of PM flux linkage vectors for α_{el}>0

$$T = \frac{3}{2} P \lambda_{PM,algn} \cos(\alpha_{el})\, i_q \tag{5}$$

In (4) and (5), P denotes the number of pole pairs, λ_{R1}, λ_{R2} are flux linkage contributions from R1, R2, and i_q, i_d are the q-axis, d-axis currents. Evidently, maximum torque is achieved when R1 and R2 are aligned.

However, it is noted that also a differential torque is developed inside the machine. Since the two rotor sections are free to rotate one with respect to the other, the differential torque will provide a shifting action that can be evaluated as:

$$T_{shift} = T_{R1} - T_{R2} = -\frac{3}{2} P \lambda_{PM,algn} \sin(\alpha_{el})\, i_d \tag{6}$$

According to (6), if R1 and R2 are already phase-shifted by α_{el} and d-axis current is applied, a differential torque is applied on R1 and R2, which can increase or decrease the existent phase-shift, depending on the sign of the d-axis current. Therefore, it is clear that the shifting of the rotors, required for MFW, can be obtained directly by the control of the d-axis current, producing a differential torque, without the need of other actuating devices. The shifting torque is of transient nature, since it is used only for providing a phase-shifting acceleration to R1 and R2. Thus, no steady-state d-axis current is necessary. Furthermore, the control of current for the flux-regulation represents a dynamically improved and reliable technique that avoids the complications of mechanical devices.

Based on (6), in order to enable the shifting torque production, it is necessary that $\alpha_{el} > 0$ at any moment. In other words, a minimum shifting angle $\alpha_{el,min}$ is required also when the machine works in the constant torque region, causing a decrease in the available torque:

$$T_{rated} = T_{rated}|_{\alpha_{el}=0} \cdot \cos(\alpha_{el,min}) \tag{7}$$

In order to ensure the minimum shifting angle, a mechanical stop is built on the shafts at $\alpha_{el.min}$. Similarly, another one is added at $\alpha_{el} = \pi/2$ when the PM flux contributions from the two rotor sections will be opposite in phase.

III. SR Machine with MFW vs Base Machine with EFW

In this section, the proposed SR machine will be compared with the corresponding base machine, equipped with a single rotor. For this comparison, the base machine taken in consideration is a 6-pole industrial SPM motor, whose nameplate parameters are listed in Table I. Let L be the axial active length of the base machine, then the SR machine model is derived by introducing two identical rotor sections having the same axial length ($L_1 = L_2$) and a spacer having axial length L_{spacer}, such that $L_1 + L_{spacer} + L_2 = L$.

The rated electromagnetic torque produced by the base SPM machine can be calculated as

$$T_{BASE} = \frac{3}{2} P \lambda_{PM_{BASE}}\, i_{BASE}. \tag{8}$$

The SR machine preserves the same no-load airgap flux density as the base machine, but the spacer airgap causes a reduction in the PM flux linkage proportional to $\left(1 - \frac{L_{spacer}}{L}\right)$, which affects torque production. On the other hand, since the stator is identical, the rated current remains the same. Therefore, when the minimum shifting angle is also considered, the rated torque of the SR machine becomes:

$$T_{rated} = \cos(\alpha_{el,min}) \left(1 - \frac{L_{spacer}}{L}\right) T_{BASE} \tag{9}$$

In order to avoid losing too much in terms of torque density, it is desirable that the length of the spacer L_{spacer} is kept at minimum. Apart from mechanical clearance requirements, however, it is noted that at high speeds the two rotor sections are strongly displaced, so that magnets of opposing polarity will be facing each other at the two sides of the spacer. Therefore, in order to avoid an excess of flux lines to be shunted between the two rotor sections, which would in turn further decrease the actual torque, it is suggested that L_{spacer} should be 3÷5 times the airgap length. For the SR machine under consideration, being the airgap equal to 1 mm, the spacer length was chosen such that $L_{spacer} = 5mm$ and therefore $\frac{L_{spacer}}{L} = 0.021$.

Similarly, the minimum phase shift angle $\alpha_{el,min}$ has a direct impact on torque production and should be as low as possible. However, the shifting torque also depends on $\alpha_{el,min}$, as well as on the d-axis current. Increasing $\alpha_{el,min}$ allows to decrease the required i_d for the same value of T_{shift}. Assuming $i_d = 0.32\ p.u.$, a value of $\alpha_{el,min} = \pi/10$ is chosen, in order to ensure a minimum shifting torque equal to approximately 10% of T_{BASE}. For the SR machine geometry, this value is enough to provide the required dynamic performance. It is important to remember that the shifting torque is required only during accelerations and that the i_d current is only transient.

TABLE I. Base Machine Parameters

Rated power	18.5 kW	Phase resistance	100 mΩ
No. of pole pairs	3	Phase inductance	3.4 mH
Rated speed	1800 rpm	Stator active length	237 mm
Rated torque	98.1 Nm	Airgap length	1 mm
Rated current	36.1 Arms		
No-load line-to-line voltage at rated speed	296 Vrms		

The achievable CPSR in SPM machines with EFW depends on the per-unit inductance, l_{pu}, and can be determined as follows [3]:

$$CPSR = \left(1 - l_{pu}\right)^{-1} \tag{10}$$

Instead, in the case of the SR machine with MFW, the CPSR does not depend on l_{pu} but on α_{el}, and is theoretically infinite, proven by substituting $\alpha_{el} = \pi/2$ in (3).

The per-unit torque vs speed characteristics of the base machine with EFW and SR machine with MFW, having the parameters listed in Table I, are shown in Fig. 6, together with the ideal characteristic. It results that the base machine provides ideal per-unit torque, but its CPSR is limited to approx. 1.7:1. From (10), the increase of l_{pu} to 0.9 would ensure the desired 10:1 CPSR. But since [3]:

$$V_{pu,rated} = \sqrt{1 + {l_{pu}}^2}, \tag{11}$$

this action would necessitate a voltage oversizing of the inverter by approx. 1.35x. A 10:1 CPSR can be achieved also by oversizing the base machine and inverter by $\frac{CPSR_{desired}}{CPSR_{actual}} \approx$ 5.9x and using the machine at reduced power. Instead, the SR machine provides the desired 10:1 CPSR for the price of a reduced nominal torque to approx. 0.93 p.u., caused by $\alpha_{el_{min}}$ and L_{spacer}. Nonetheless, the SR machine with MFW can guarantee the ideal characteristic for a machine oversizing of approx. 1.07x, which is the smallest value among the previously given alternatives.

IV. Finite Element Results

A 3D model of the split rotor SPM machine described in section III is created in Simcenter MagNet®, for finite element analysis (FEA).

a) Correspondence with the theoretical results

The mechanical flux-weakening and the influence of L_{spacer} on the total PM flux-linkage is verified through static 3D FEA. Preliminarily, the flux density amplitude at the airgap, in proximity of the spacer, is investigated. Fig. 7 shows the results of the simulation in the worst condition, i.e. when the phase shifting angle between the rotor sections is $\alpha_{el} = \pi/2$, which implies that permanent magnets of opposing polarity are facing at the spacer. Despite that, it is clearly shown how the airgap flux density amplitude drops practically to zero in correspondence to the spacer, meaning that the flux leakage between the two rotor sections is negligible and therefore they can be considered as independent from each other.

The per-unit ($\frac{\lambda_{PM}}{\lambda_{PM,BASE}}$) PM flux linkage values from FEA and from (1), as a function of the electrical phase-shift, are plotted in Fig. 8. The simulation confirms the reduction in the flux linkage due to the effect of the spacer with the coefficient $\left(1 - \frac{L_{spacer}}{L}\right)$. For the present choice of the spacer length and for aligned rotor sections the flux linkage is 98% of the base machine. A very good agreement between the FEA and the theoretical predictions can be observed in Fig. 8 also for different values of the shifting angle α_{el}.

The motoring and the shifting torque are also investigated for different values of α_{el} and the related graphs are reported in Figs. 9 and 10. Again, a very good agreement is found between the simulations and the analytical predictions from (5) and (6) respectively.

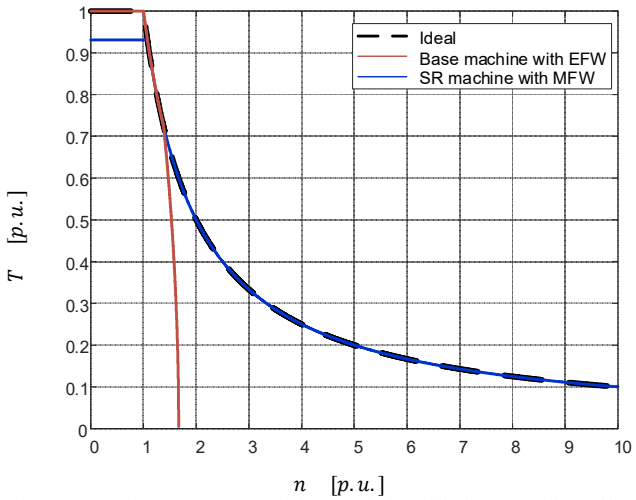

Fig. 6. Per-unit torque vs speed characteristic of the base machine with EFW and SR machine with MFW.

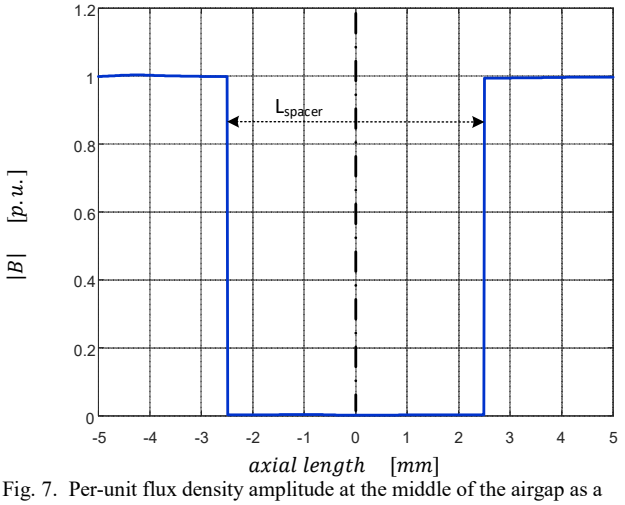

Fig. 7. Per-unit flux density amplitude at the middle of the airgap as a function of the axial length, in proximity of the spacer

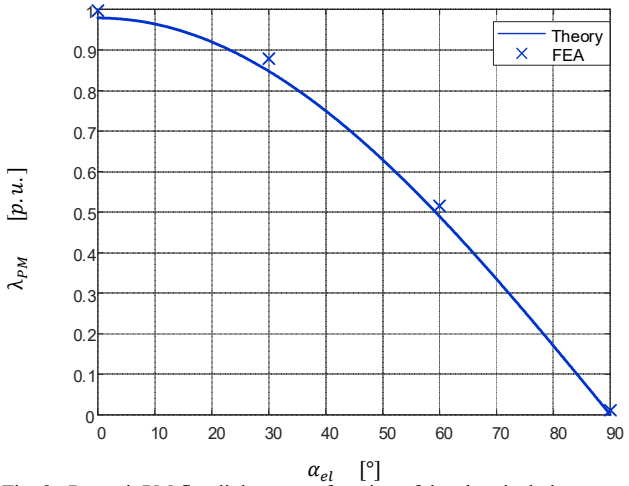

Fig. 8. Per-unit PM flux linkage as a function of the electrical phase-shift, from theory and FEA, for $\frac{L_{spacer}}{L} = 0.021$

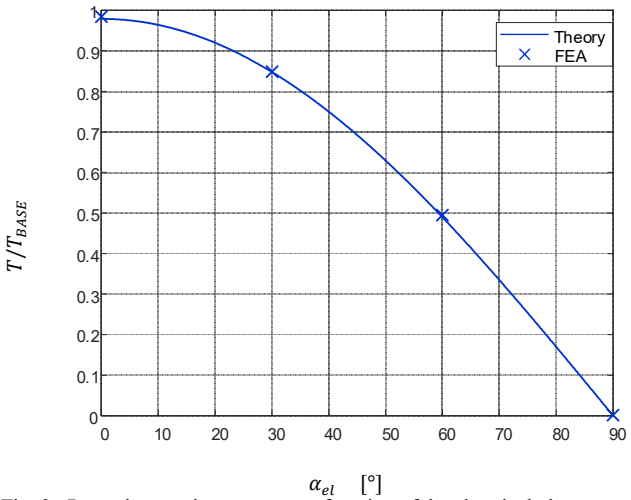

Fig. 9. Per-unit motoring torque as a function of the electrical phase-shift, from prediction and FEA solutions, for $i_q = i_{BASE}$

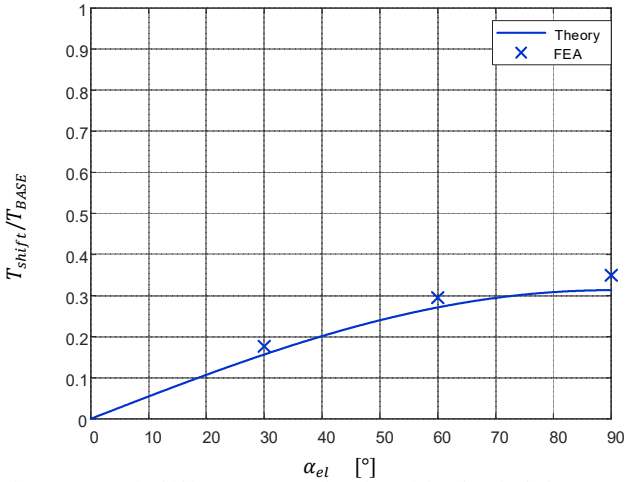

Fig. 10. Per-unit shifting torque as a function of the electrical phase-shift, from prediction and FEA solutions, for $i_d = 0.32\ i_{BASE}$

b) Induced Voltage Waveforms

Until this point, it was assumed that the flux linkage distribution is purely sinusoidal. This is not true in practice, since the airgap flux density waveform contains spatial harmonics that are mainly dependent on the geometry of the PMs and of the stator slots/teeth. In turn, these harmonics will reflect in the induced voltage waveforms. At low speed, their effect is usually insignificant.

Once field weakening region is entered, the phase-shift between the rotor discs can be controlled according to (3) in order to keep the induced voltage constant, but only to the extent of the fundamental component. In other words, the MFW does not allow to control the amplitude of the higher order components, since their phase-shift angle is given not only by α_{el} but also by the harmonic order. For this reason, their effect after base speed needs to be properly investigated.

Measures that can be adopted in order to reduce the harmonic content in the flux linkage are widely known and the base machine that is taken as a reference for the SR design already implements some of them. In fact, the stator winding is divided into 2 slots/pole/phase (for a total of 36 slots) with full pitch coils. In addition, the stator is skewed by one slot pitch. The SR machine retains the same stator, but since now the rotor is split in two sections, each of them having half of the total axial length (the impact of the spacer can be neglected in this analysis), the result is that each rotor section will see a skewing for only half of the slot pitch. As a consequence, each rotor section is designed with an additional skewing of another half of the slot pitch, which can be appreciated in the drawings of Figs. 3 and 4.

Fig. 11 shows the no load phase voltage calculated at the base speed and assuming the two rotor sections aligned ($\alpha_{el} = 0$). The dotted curve represents the case where no skewing at all is present, while the continuous one corresponds to the above-described case of one slot pitch skewing distributed between the stator and each rotor section.

While Fig. 11 demonstrates that the skewing is very effective, as expected from theory, in cutting down the 7th, 11th, 13th and partially also the 5th, it is also clear that the 3rd harmonic remains almost unaltered. This becomes more and more evident as the speed increase and the MFW mechanism keeps constant the fundamental component only. Fig. 12 shows this phenomenon clearly, plotting the no load phase voltage at different speeds for $n = 2; 3; 5; 10\ p.u.$, and with the shifting angle α_{el} calculated as in (3). Comparison with the induced voltage at rated speed (and no phase shifting), already shown in Fig. 11, highlights the increased contribution of the 3rd harmonic with the frequency.

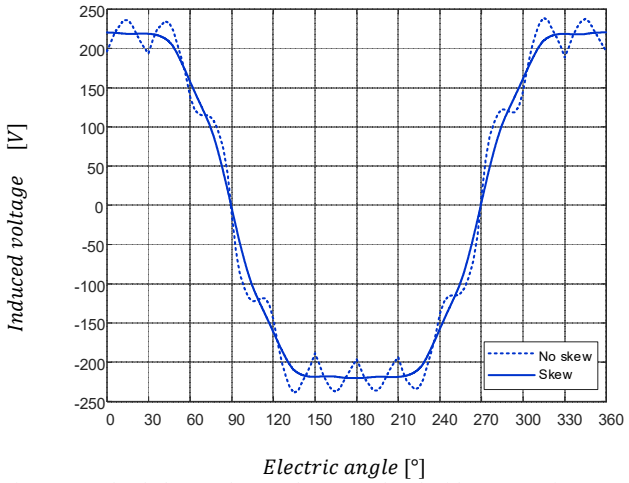

Fig. 11. No load phase voltage at base speed and with rotor sections aligned: no skewing (dotted) and skewing (continuous).

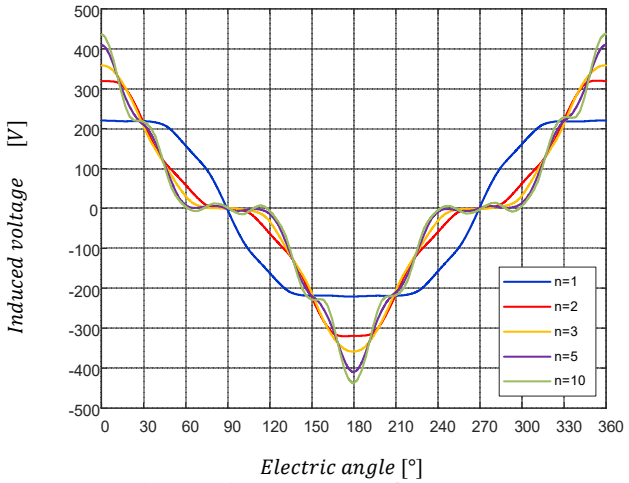

Fig. 12. No load phase voltage, at $n = 2\ (red)$; 3 $(orange)$; 5 $(purple)$, 10 $(green)$ $p.u.$ and with shifting angle α_{el} according to (3). Comparison with waveform at $n = 1\ (blue)$ in Fig. 11.

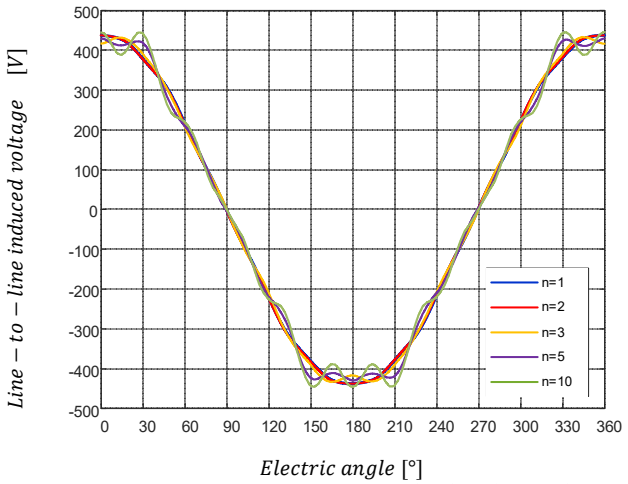

Fig. 13. No load line-to-line voltage, at $n = 2$ (red); 3 $(orange)$; 5 $(purple)$, 10 $(green)$ $p.u.$ and with shifting angle α_{el} according to (3). Comparison with waveform at $n = 1$ $(blue)$.

On the other side, however, it has to be noted that the voltage constraint in the CPSR is determined by the comparison of the dc link amplitude (generally constant) and the line-to-line voltage. Therefore, Fig. 13 shows also the comparison of the line-to-line no load voltages for the same speeds and shifting angles as in Fig. 12. It is evident how, despite the 10:1 ratio in the frequency, the peak-to-peak value remains constant and the harmonic content extremely limited.

c) Losses and Efficiency

Whenever electrical machines are required to operate at high speeds, such as in the case of a very wide CPSR, iron and PM losses always need to be carefully considered, since they increase more than linearly with frequency. The fundamental frequency at rated speed of the SR machine is 90 Hz and, considering a 10:1 CPSR, a maximum frequency of 900 Hz is obtained. At these fundamental frequencies, harmonics of the flux density distribution will also play a significant role in the total losses, even though small in amplitude. Furthermore, it is recognized in [6] that MFW allows to reduce the flux linkage with the windings as the speed increases, but does not act of the flux density. As a result, while in machines with EFW iron losses can generally be considered almost constant, in the MFW case this is not true and losses are expected to increase with the frequency.

Finite element transient with motion FEA were used in order to evaluate no load losses inside the machine at various frequencies along the CPSR. In particular, results obtained at $n = 1; 2; 3; 5; 10\ p.u.$ are presented here. At each speed, the two rotor sections are shifted by the angle α_{el} calculated from (3).

Figure 14 shows the per-unit losses in the stator iron, as a function of the frequency, both as a whole and split among hysteresis and eddy currents losses, so that the relevance of the two contributions can be appreciated. M235-35A laminated steel is used in the stator iron. The diagram shows that eddy currents losses become predominant at a speed of 7 p.u. It is important to remember that this is not an optimized design and that the stator, for comparison purposes, is kept identical to the base SPM machine. However, this latter was designed for a maximum frequency that did not exceed 180Hz, while the SR machine reaches 900 Hz at $n = 10\ p.u.$

Rotor losses too have been evaluated, considering the rotor yoke made of pure iron, with no lamination, and no segmentation in the PMs. Despite the lack of lamination, FEA results show that the losses in the rotor iron are negligible. Not the same, unfortunately, can be said for the losses in the PMs, as it is evident from Fig. 15. Without segmentation, these losses actually exceed stator iron losses in a speed range from 5 p.u. to 10 p.u. Considering that heat extraction from the rotor is always a bigger challenge, it follows that segmentation is required. It is therefore decided to perform axial segmentation subdividing each magnet in each rotor section into 7 axial segments. Another simulation is then run at 10 p.u. speed to evaluate losses in this configuration. It is found that they are cut down almost to half, consistently to what can be found in literature [24]. Therefore, the actual PM losses are expected to lie along the dotted gray curve in Fig. 15. Again, it needs to be underlined that proper optimization can lead to a further significant reduction in those losses.

Finally, Joule losses can be calculated from the data in Table I and the expected efficiency at rated current is plotted as in Fig. 16, when the effect of PM segmentation is not considered. Even under this detrimental hypothesis, the efficiency is expected to be around 97% at the corner point (rated power) and around 86% in the CPSR at 5 p.u. speed.

The effect of PM segmentation on the efficiency is expected to be more consistent in the CPSR between 5 and 10 p.u. speed. For example, at 10 p.u., the expected efficiency should rise from 56% to 66%.

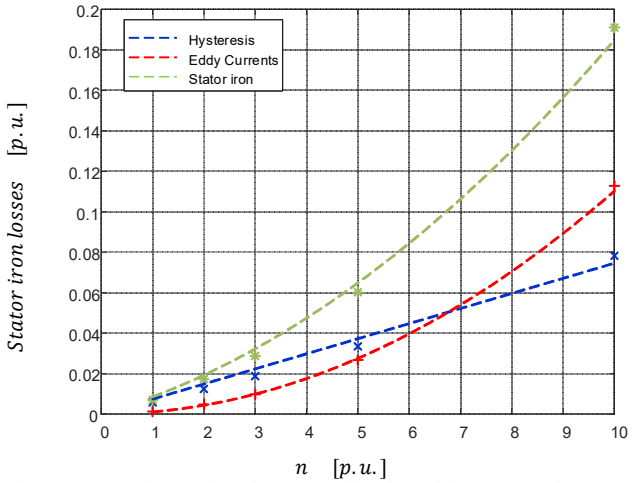

Fig. 14. Per-unit stator iron losses as a function of frequency, when MFW is applied according to (3)

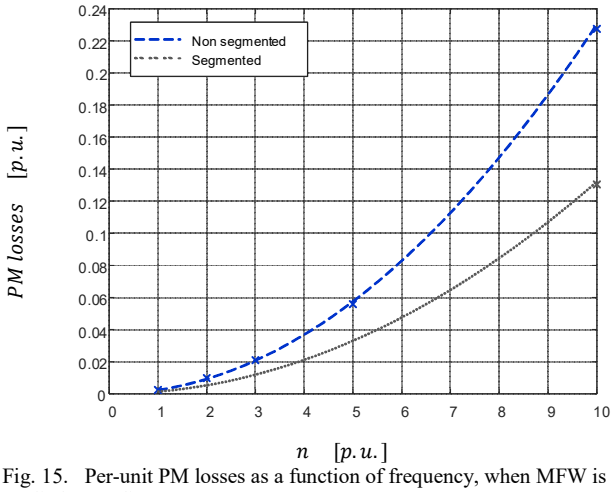

Fig. 15. Per-unit PM losses as a function of frequency, when MFW is applied according to (3)

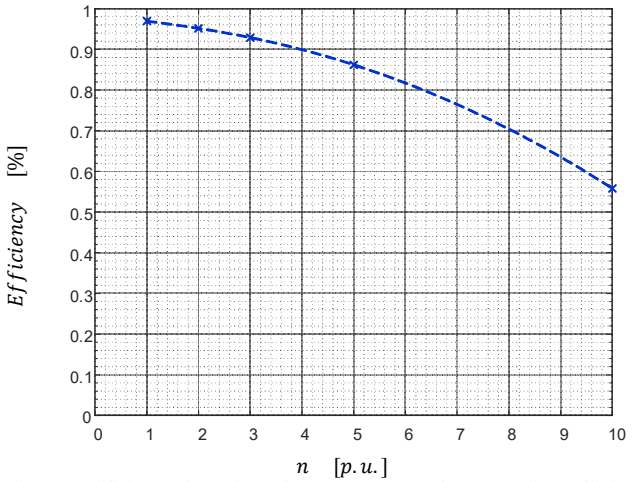

Fig. 16. Efficiency throughout the CPSR range, when MFW is applied according to (3). PM segmentation not considered.

V. Conclusions and Future Work

A split rotor SPM machine in which the MFW is achieved through an internal electromagnetic shifting torque, without any external device, was presented. Control of the shifting torque is obtained through the d-axis current. The analysis demonstrated that the proposed machine could provide a 10:1 CPSR, at the expense of a very small decrease in the torque density compared to the base SPM machine. Special attention is required in the design phase in order to reduce the harmonic content of the airgap flux density and the frequency dependent losses inside the machine. A prototype of the SR machine is currently under construction, in order to experimentally verify the predictions coming from theory and simulations. Further aspects regarding the dynamics of the phase-shifting control are currently under development.

References

[1] B. Lequesne, "Automotive Electrification: The Nonhybrid Story," *IEEE Trans. Transport. Electrific.*, vol. 1, no. 1, pp. 40-53, June 2015.

[2] A. M. EL-Refaie and T. M. Jahns, "Optimal flux weakening in surface PM machines using fractional-slot concentrated windings," in *IEEE Transactions on Industry Applications*, vol. 41, no. 3, pp. 790-800, May-June 2005, doi: 10.1109/TIA.2005.847312.

[3] F. Giulii Capponi, G. Borocci, G. De Donato and F. Caricchi, "Flux Regulation Strategies for Hybrid Excitation Synchronous Machines," in *IEEE Transactions on Industry Applications*, vol. 51, no. 5, pp. 3838-3847, Sept.-Oct. 2015, doi: 10.1109/TIA.2015.2417120.

[4] T. M. Jahns, G. B. Kliman and T. W. Neumann, "Interior PermanentMagnet Synchronous Motors for Adjustable-Speed Drives," in *IEEE Transactions on Industry Applications*, vol. IA-22, no. 4, pp. 738-747, July 1986, doi: 10.1109/TIA.1986.4504786.

[5] N. Bianchi, S. Bolognani and B. J. Chalmers, "Salient-rotor PM synchronous motors for an extended flux-weakening operation range," in *IEEE Transactions on Industry Applications*, vol. 36, no. 4, pp. 1118-1125, July-Aug. 2000, doi: 10.1109/28.855968.

[6] F. Giulii Capponi, G. De Donato, G. Borocci and F. Caricchi, "Axial-Flux Hybrid-Excitation Synchronous Machine: Analysis, Design, and Experimental Evaluation," in *IEEE Transactions on Industry Applications*, vol. 50, no. 5, pp. 3173-3184, Sept.-Oct. 2014, doi: 10.1109/TIA.2014.2303253.

[7] J. Cekani, F. G. Capponi, G. De Donato and F. Caricchi, "Mechanical Flux Weakening Methods for the Achievement of a Very Wide Constant Power Speed Range in Automotive Applications," *IEEE JESTPE*, early access, doi: 10.1109/JESTPE.2021.3058198.

[8] Y. Wang, C. Li and T. Meng, "Research on electromagnetic force for a self-adaptive passive flux-weakening PMSM," 2019 22nd International Conference on Electrical Machines and Systems (ICEMS), 2019, pp. 1-5, doi: 10.1109/ICEMS.2019.8921664.

[9] Ma, Lei & Sanada, Masayuki & Morimoto, Shigeo & Takeda, Yoji. (2001). IPMSM with Adjustable PM Armature Flux Linkage for High Efficiency and Wide Range Operation. *IEEJ Transactions on Industry Applications*. 121. 371-376. 10.1541/ieejias.121.371.

[10] N. Elloumi, M. Bortolozzi, A. Masmoudi, M. Mezzarobba, M. Olivo and A. Tessarolo, "Numerical and Analytical Approaches to the Modeling of a Spoke Type IPM Machine with Enhanced Flux Weakening Capability," in *IEEE Transactions on Industry Applications*, vol. 55, no. 5, pp. 4702- 4714, Sept.-Oct. 2019.

[11] I. Urquhart, D. Tanaka, R. Owen, Z. Q. Zhu, J. B. Wang and D. A. Stone, "Mechanically actuated variable flux IPMSM for EV and HEV applications," 2013 World Electric Vehicle Symposium and Exhibition (EVS27), Barcelona, 2013, pp. 1-12.

[12] Z. Q. Zhu, M. M. J. Al-Ani, X. Liu, M. Hasegawa, A. Pride and R. Deodhar, "Comparison of flux weakening capability in alternative switched flux permanent magnet machines by mechanical adjusters," 2012 XXth International Conference on Electrical Machines, Marseille, 2012, pp. 2889- 2895.

[13] J. Yang, Q. Li, Y. Feng, P. Liu, S. Huang and L. Wang, "Simulation and Experimental Analysis of a Mechanical Flux Modulated Permanent Magnet Homopolar Inductor Machine," in *IEEE Transactions on Transportation Electrification*, vol. 8, no. 2, pp. 2629-2639, June 2022, doi: 10.1109/TTE.2022.3140602.

[14] S. Roggia, G. Roggia and A. Gimeno, "Adjustable air gap machine for aerospace applications," 2020 International Conference on Electrical Machines (ICEM), 2020, pp. 599-605, doi: 10.1109/ICEM49940.2020.9270902.

[15] Wang, S., Lu, J., Li, B. *et al.* Design and analysis of mechanical flux-weakening device of axial flux permanent magnet machines. *J. Power Electron.* 22, 653–663 (2022). https://doi.org/10.1007/s43236-022-00386-1

[16] Joel B. Jermakian, Stephen G. Crain, Cory D. Knudtson, Robert F. D. Piacesi, "Electric motor with active hysteresis-based control of winding currents and/or having an efficient stator winding arrangement and/or adjustable airgap", US 6348751B1, Feb. 19, 2002. https://patents.google.com/patent/US6348751?oq=US+6%2c348%2c751+ B1

[17] Lei Hao, Chandra S. Namuduri, "Variable geometry electric machine", US 20110101817 A1, May 5, 2011. https://patentimages.storage.googleapis.com/b2/c0/86/ac1417b300d4d1/US 20110101817A1.pdf

[18] Oh, Sung & Kern, Justin & Bohn, T. & Rousseau, Aymeric & Pasquier, Maxime. (2002). Axial Flux Variable Gap Motor: Application in Vehicle Systems. 10.4271/2002-01-1088.

[19] L. Del Ferraro, F. Caricchi, F. G. Capponi and G. De Donato, "Axial-flux PM starter/alternator machine with a novel mechanical device for extended flux weakening capabilities," Conference Record of the 2004 IEEE Industry Applications Conference, 2004. 39th IAS Annual Meeting., 2004, pp. 1413-1419 vol.3, doi: 10.1109/IAS.2004.1348607.

[20] F. Giulii Capponi, R. Terrigi, F. Caricchi and L. Del Ferraro, "Active Output Voltage Regulation for an Ironless Axial-Flux PM Automotive Alternator with Electromechanical Flux Weakening," *IEEE Trans. Ind. Appl.*, vol. 45, no. 5, pp. 1785-1793, Sept.-oct. 2009.

[21] X. Liu, M. Wang, D. Chen and Q. Xie, "A Variable Flux Axial Field Permanent Magnet Synchronous Machine With a Novel Mechanical Device," in *IEEE Transactions on Magnetics*, vol. 51, no. 11, pp. 1-4, Nov. 2015, Art no. 8113504, doi: 10.1109/TMAG.2015.2450501.

[22] Jing Zhao, Bin Li, and Zhongxin Gu. "Research on an Axial Flux PMSM with Radially Sliding Permanent Magnets" *Energies*, vol. 8, no. 3, 2015. doi:10.3390/en8031663

[23] M. C. Kulan, N. J. Baker and S. Turvey, "Split Rotor Concept for Permanent Magnet Electrical Machines," 2019 IEEE International Electric Machines & Drives Conference (IEMDC), San Diego, CA, USA, 2019, pp. 700-707.

[24] J. D. Ede, K. Atallah, G. W. Jewell, J. B. Wang and D. Howe, "Effect of Axial Segmentation of Permanent Magnets on Rotor Loss in Modular Permanent-Magnet Brushless Machines," in *IEEE Transactions on Industry Applications*, vol. 43, no. 5, pp. 1207-1213, Sept.-oct. 2007, doi: 10.1109/TIA.2007.904397.